Size dependence of exciton fine structure in CdSe quantum dots

D. J. Norris*
Massachusetts Institute of Technology, 77 Massachusetts Avenue, Cambridge, Massachusetts 02139

Al. L. Efros and M. Rosen
Beam Theory Section, Naval Research Laboratory, Washington, D.C. 20375

M. G. Bawendi
Massachusetts Institute of Technology, 77 Massachusetts Avenue, Cambridge, Massachusetts 02139

(Received 18 July 1995)

We use photoluminescence excitation and fluorescence line narrowing spectroscopies to examine structure observed in the band-edge absorption feature of CdSe quantum dots. We study eight samples ranging from ~15 to ~50 Å in radius to probe the size dependence of this structure. We compare our results with recent theories, which predict band-edge exciton splittings in CdSe dots due to their internal crystal structure, nonspherical shape, and the exchange interaction between the electron and hole. We find reasonable agreement between our data and theory, supporting the observation of exciton fine structure. [S0163-1829(96)07220-7]

I. INTRODUCTION

Nanometer-scale semiconductor crystallites (or quantum dots) provide an opportunity to investigate excitons that are confined in all three dimensions. In these so-called zero-dimensional materials an electron-hole pair generated by optical absorption is spatially confined by the quantum dot (QD) boundary. If the QD's are small compared to the exciton Bohr radius, they exhibit optical properties that differ dramatically from the bulk material. The bulk valence and conduction bands are quantized and discrete transitions, which increase in energy with decreasing size, appear in the QD spectrum.[1–3] This is demonstrated in the preceding paper where a series of high-quality CdSe quantum dot samples are used to follow the size evolution of ten transitions in the QD optical spectrum.[4] In general these absorption features are well described by QD effective mass models, which incorporate the complexities of the CdSe valence band.[5–9] However, while these models predict that the lowest-energy electron-hole pair state ($1S_{3/2}1S_e$—which we refer to as the ''band-edge exciton'') is eightfold degenerate, we also observe structure within the first absorption feature of our samples. Such a structure has been predicted to arise in the band-edge exciton due to the nonspherical shape and internal crystal structure of our dots,[10,11] which are slightly prolate with a wurtzite lattice.[12] Both effects should split the band-edge exciton into two fourfold degenerate states, analogous to the bulk ''*A*-*B* splitting.'' [10,11] In addition the exchange interaction between the electron and hole should strongly modify the band-edge exciton structure.[13–16] The exchange splitting, while negligible in the bulk, should be strongly enhanced by quantum confinement.[13–16] When all of these effects are combined, the resulting band-edge structure has important implications for QD optical behavior. For example, the lowest QD level is predicted to be optically forbidden and this may explain the long (~1 μs at 10 K) radiative lifetimes observed in these systems.[14–16]

To further test these models, in this paper we present the size dependence of the band-edge absorption structure in CdSe QD's. Previously we reported the band-edge structure of a ~30-Å effective radius[17] sample using transient differential absorption (TDA) spectroscopy.[18] This technique reduces residual sample inhomogeneities present in even the highest-quality QD samples. Here we use two simpler optical methods, photoluminescence excitation (PLE) and fluorescence line narrowing (FLN) spectroscopies, to reduce inhomogeneities and obtain absorption and emission information for each sample in our size series. Our data support our previous conclusion[18] that the absorption structure is the band-edge exciton fine structure predicted by theory.[10,11,13–16]

II. EXPERIMENT

We study eight CdSe samples (A–H) with mean effective radii ranging from ~15 Å (A) to ~50 Å (H).[17] The samples are similar to those described in the preceding paper.[4] The dots have a wurtzite lattice and are prolate with an aspect ratio ranging between 1.0 and 1.3, increasing with dot size.[12,19] The long axis is parallel to the unique ''*c*'' axis of the wurtzite crystal.

For optical measurements five of the samples were isolated from their growth solution and redispersed in *n*-hexane with a small amount of tri-*n*-octyl-phosphine added. The remaining three, which were prepared to obtain absorption as well as PLE and FLN data, were redispersed in tri-*n*-butyl-phosphine with *o*-terphenyl added (250 mg/ml) to form an optically clear organic glass at cryogenic temperatures. We find no difference between these two solvent mixtures in our results. Each sample solution is sealed between sapphire flats separated by a 0.5-mm-thick Teflon spacer and mounted in a helium cryostat. All spectra are obtained at 10 K using a Spex Fluorolog-2 spectrofluorometer with a typical resolution of ~1.5 meV (full width at half maximum).

III. RESULTS

Figure 1(a) shows absorption and emission results for sample (B) (~19-Å effective radius). The emission spec-

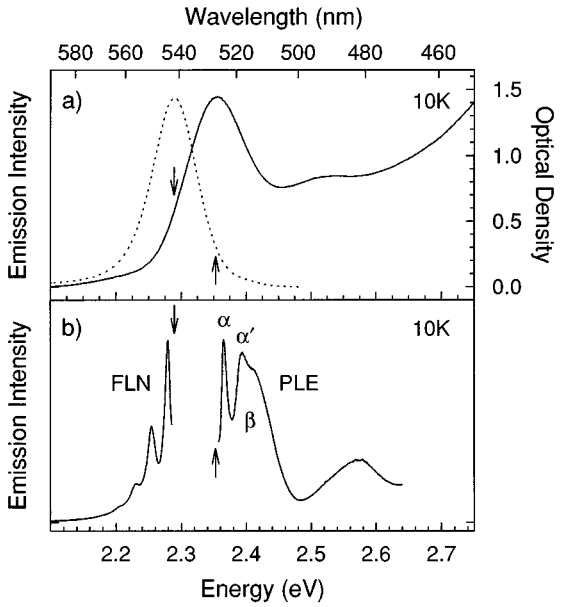

FIG. 1. (a) Absorption (solid line) and full luminescence (dotted line) spectra for sample B, ~19 Å effective radius. (b) FLN and PLE spectra for sample B. A LO-phonon progression is observed in FLN. Both narrow (α,α') and broad (β) absorption features are resolved in PLE. The downward (upward) arrows denote the excitation (emission) position used for FLN (PLE).

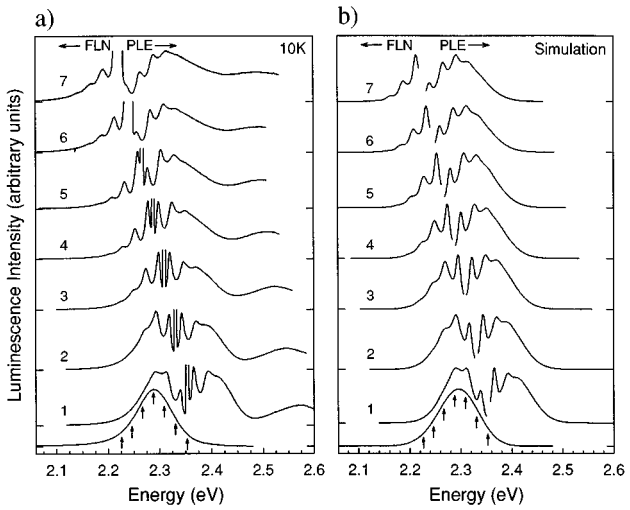

FIG. 2. (a) Normalized FLN and PLE data for sample B for various excitation and emission positions. For each FLN-PLE pair, the FLN excitation and PLE emission energies are the same. These energies are designated by arrows and shown with the full luminescence. FLN emission becomes sufficiently weak in curves 6 and 7 that the zero-phonon line of the emitting state is obscured by scattered excitation light. (b) Simulation of FLN-PLE spectra for sample B as in (a).

trum, referred to as ''full luminescence,'' is obtained by exciting the sample well above its first transition so that emission occurs from the entire sample distribution. While no structure is observed within the band-edge absorption and emission features, residual sample inhomogeneities conceal band-edge spectral features. FLN and PLE spectroscopies, demonstrated in Fig. 1(b), can provide higher resolution and reveal band-edge structure.[20] In FLN a subset of the sample distribution is optically excited, revealing a significantly narrowed and structured spectrum. For example, when sample B is excited on the low-energy side of its first absorption feature (downward arrows in Fig. 1) a longitudinal optical (LO) phonon progression is clearly resolved. This FLN spectrum can be used to extract a model ''single dot'' emission line shape.[21] PLE can be used similarly to extract ''single dot'' absorption information by monitoring a narrow spectral band (upward arrows) of the full luminescence while scanning the excitation energy.[4,20,22–24] As seen in Fig. 1(b), additional structure in the first absorption feature is resolved with this technique. A narrow feature (α), its LO-phonon replica (α'), and a broader feature (β) are observed.

For a particular sample, the overall shape of the band-edge PLE structure depends on where we monitor the full luminescence. Similarly, FLN results depend on the excitation position. For example, Fig. 2(a) shows seven FLN and PLE scans for sample B. For each pair of FLN-PLE results (numbered 1–7) the FLN excitation energy and PLE emission energy are identical. These energies are represented by arrows and shown with the full luminescence. As the PLE emission position is moved to lower energy (from 1 to 7), the broad underlying feature (β) broadens and additional phonon replicas of the narrow feature (α) appear. The highest resolution in PLE is thus obtained when the emission is monitored on the blue edge of the full luminescence, probing the ''smallest'' dots in the distribution.[20,25] In contrast to PLE, the FLN spectra broaden as the excitation position is moved to higher energy, eventually approaching the full luminescence in curve one. The highest resolution in FLN is obtained by exciting the sample on the red edge of the first absorption feature, probing the ''largest'' dots in the distribution.[20,25]

These trends originate in the inhomogeneous sample distribution. In FLN, the single dot emission line shape is convoluted with unwanted absorption information. Any dot that has an absorption feature at the excitation energy is excited. In PLE, the single dot absorption line shape is convoluted with unwanted emission information. The PLE experiment simultaneously monitors dots that emit from different LO-phonon lines. In both cases, the fractions of dots that have a particular absorption feature or phonon line at the excitation or emission position are determined by the sample distribution. However, despite this contamination of the PLE and FLN results, single dot absorption and emission line shapes[21] can be extracted from a complete data set such as that in Fig. 2(a). For each sample in our size series (A–H) we record a similar FLN-PLE data set. Here we present complete and representative sets for samples B [Fig. 2(a)] and G (Fig. 3). The remainder are shown in Ref. 26.

The complete data set for sample G is shown in Fig. 3 to demonstrate the particularly interesting band-edge structure that develops in larger dots. Figure 4 shows curve 2 from Fig. 3 in more detail. Although the spectra for sample G (Fig. 4) appear more complex than for sample B [Fig. 1(b)], the primary difference is that the broad absorption feature [β in Fig. 1(b)] is now split into two features (β_1 and β_2 in Fig. 4). In addition the linewidths of β_1 and β_2 are comparable to the linewidth of α. In other words, while in sample B three

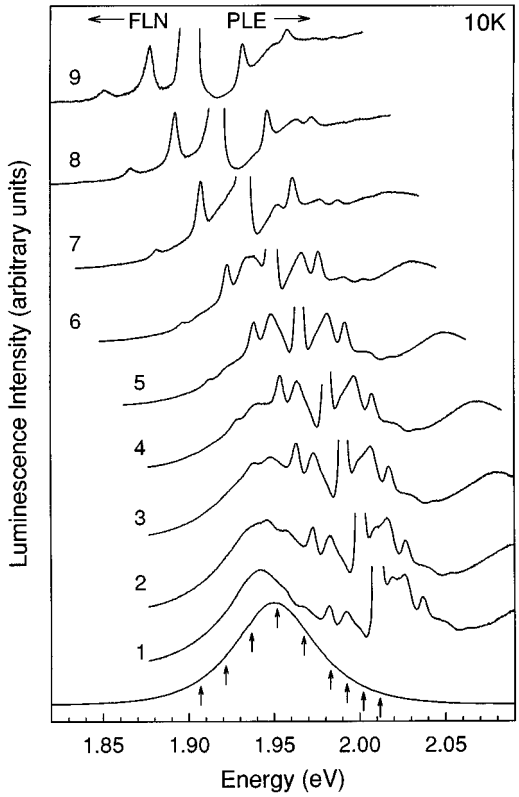

FIG. 3. Normalized FLN and PLE data for sample G (~44 Å effective radius) as in Fig. 2. For each FLN-PLE pair, the FLN excitation and PLE emission energies are the same. These energies are designated by arrows and shown with the full luminescence.

band-edge states are resolved [a narrow emitting state, a narrow absorbing state (α), and a broad absorbing state (β)], in sample G four band-edge states are present [a narrow emitting state and three narrow absorbing states (α, β_1, and β_2)]. Although the emission still arises from a single LO-phonon progression, as indicated by curve 9 in Fig. 3, the absorption structure causes three overlapping phonon progressions to appear in the FLN and PLE results in Fig. 4. Each progression can be assigned to one of the three absorbing features (horizontal brackets in Fig. 4). For example, the FLN feature labeled β_2 and its replica are observed because of absorption by a subset of dots into β_2 followed by relaxation into the emitting state. We note that since the separation between α and the emitting state (the Stokes shift) is ~1 meV in dots of this size, the zero-phonon line of α is obscured by scattered excitation light in PLE. Similarly, in FLN the zero-phonon line of the emitting state is obscured for those dots that absorb directly into α. However, higher replicas due to α are clearly observed in both FLN and PLE.

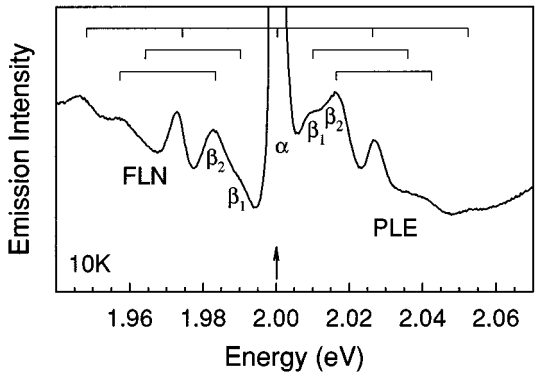

FIG. 4. Detail of FLN and PLE data for sample G (curve 2 from Fig. 3). Although emission arises from a single emitting state and its LO-phonon replicas, three overlapping LO-phonon progressions are observed in FLN due to the three band-edge absorption features (α, β_1, and β_2). Horizontal brackets connect the FLN and PLE features with their LO-phonon replicas. The arrow denotes both the FLN excitation and PLE emission energies (2.000 eV).

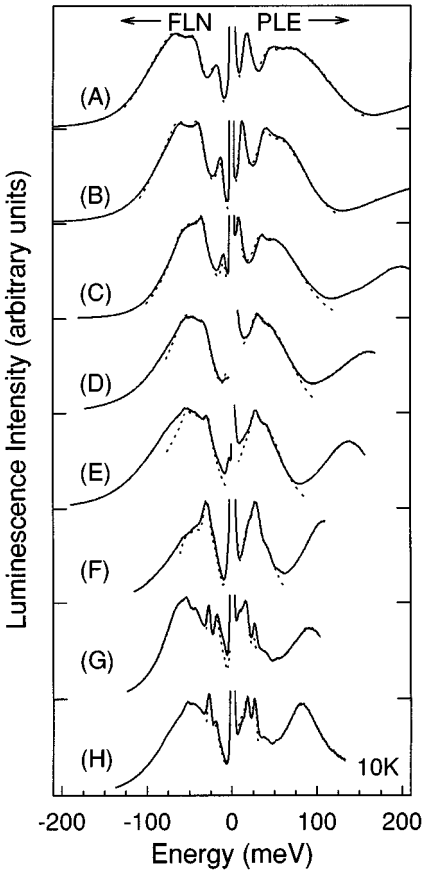

FIG. 5. The size dependence of band-edge FLN-PLE spectra. In each pair of FLN-PLE results (solid lines) the FLN excitation and the PLE emission energies are the same and indicated by arrows in the full luminescence spectra in Fig. 6. For each sample the PLE spectrum with the highest resolution is shown. The PLE (FLN) data are plotted relative to the emission (excitation) energy. Dotted lines show the best fit obtained by the global fitting procedure. For samples A-E nine parameters were adjusted: $\gamma_{1,0}$, $\gamma_{2,0}$, γ_d, ν_0, δ_1, δ_2, C_2/C_1, S_a, and S_e. For samples F-H three more parameters were required: $\gamma_{3,0}$, δ_3, and C_3/C_1. We assume that $\omega_{\mathrm{LO}}=26$ meV,[41] $\gamma_0=\gamma_{1,0}$,[45] and $\gamma_{n(l,m)}=1.5\gamma_{0(l,0)}$ for $n\neq 0$ in emission ($m\neq 0$ in absorption).

The size evolution of the band-edge structure is shown in Fig. 5, which compares FLN-PLE results for each sample in our series. The PLE spectrum with the highest resolution is shown. For each FLN-PLE pair the FLN excitation and PLE emission energies are the same and the data are plotted relative to this energy. The actual excitation-emission positions are indicated with arrows in the full luminescence spectra, shown in Fig. 6.

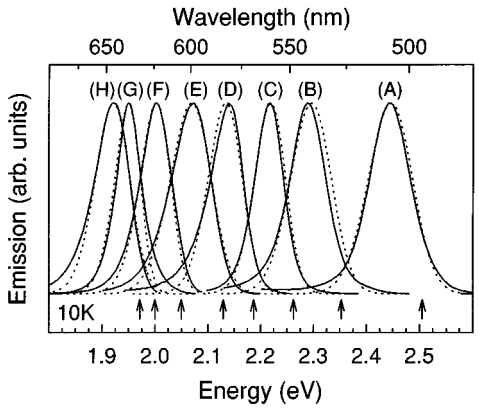

FIG. 6. Full luminescence spectra for our size series (solid lines). Arrows indicate the FLN excitation positions and PLE emission positions (eV) used in Fig. 5: (A) 2.505, (B) 2.353, (C) 2.263, (D) 2.187, (E) 2.129, (F) 2.050, (G) 2.000, and (H) 1.971. Dotted lines show the best fit obtained by the global fitting procedure.

From Fig. 5 we determine the underlying band-edge structure by simulating the FLN and PLE results. The FLN and PLE emission signals (E_{FLN} and E_{PLE}) are convolutions of the single dot absorption cross section (A), the single dot emission line shape (E), and a probability distribution function (D). D incorporates the various contributions, such as size and shape variations, to the inhomogeneous broadening and indicates what fraction of the sample emits at a particular energy. Following Ref. 27 we evaluate the convolution integrals,

$$\left.\begin{matrix} E_{\mathrm{FLN}}(\upsilon_{\mathrm{em}})|_{\upsilon_{\mathrm{exc}}} \\ E_{\mathrm{PLE}}(\upsilon_{\mathrm{exc}})|_{\upsilon_{\mathrm{em}}} \end{matrix}\right\} = C\int A(\upsilon_{\mathrm{exc}},\upsilon')E(\upsilon_{\mathrm{em}},\upsilon')D(\upsilon',\upsilon_0)d\upsilon', \tag{1}$$

where the emission and excitation positions (υ_{em} and υ_{exc}) are fixed in FLN and PLE, respectively. C is a constant with the appropriate units, which incorporates experimental parameters. We assume that $D(\upsilon',\upsilon_0)$ is a normalized Gaussian centered at υ_0 with linewidth γ_d, and that

$$A(\upsilon_{\mathrm{exc}},\upsilon') = \sum_{l=1}^{2\ \text{or}\ 3}\sum_{m=0}^{2}\frac{C_l}{\sqrt{2\pi\gamma_{l,m}^2}}\frac{(S_a)^m}{m!} \times\exp\left(-\frac{[\upsilon_{\mathrm{exc}}-(\upsilon'+\delta_l+m\omega_{\mathrm{LO}})]^2}{2\gamma_{l,m}^2}\right), \tag{2}$$

$$E(\upsilon_{\mathrm{em}},\upsilon') = \sum_{n=0}^{4}\frac{1}{\sqrt{2\pi\gamma_n^2}}\frac{(S_e)^n}{n!} \times\exp\left(-\frac{[\upsilon_{\mathrm{em}}-(\upsilon'-n\omega_{\mathrm{LO}})]^2}{2\gamma_n^2}\right), \tag{3}$$

where υ' is the position of the zero-phonon line in emission. The absorption line shape includes either two (samples A–E) or three (F–H) absorbing states, each shifted δ_l, from υ' and with integrated area C_l. Thus δ_1 is the Stokes shift between the lowest absorbing state and the emitting state. $S_{a(e)}$ is the exciton-LO-phonon coupling strength in absorption (emission) and, assuming a displaced Harmonic-oscillator model

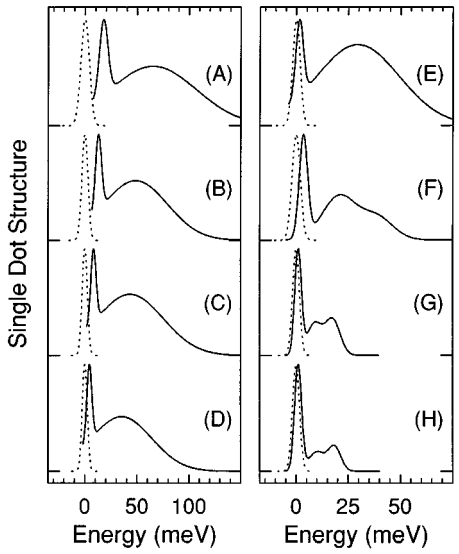

FIG. 7. Single dot absorption (solid lines) and emission (dotted lines) structure for samples A-H required to fit the FLN-PLE data in Figs. 5 and 6. The positions are shown relative to the emitting state. For clarity the LO-phonon replicas are not included. Note the factor of 2 difference in energy axes between samples A–D and E–H.

for LO-phonon coupling, is equivalent to the Huang-Rhys parameter.[28,29] We consider the first five (three) LO-phonon replicas in emission (absorption), separated by ω_{LO}, the LO phonon frequency. The nth (mth) replica of the emitting (lth absorbing) state has linewidth $\gamma_{n(l,m)}$. Within each sample distribution we assume that A and E are fixed.

For each sample we reproduce the FLN, PLE, and full luminescence[30] data from Figs. 5 and 6 using Eqs. (1)–(3). The parameters are varied using standard nonlinear least-squares methods.[31] The best fits obtained are shown as dotted lines in Figs. 5 and 6. The complete FLN/PLE data set for each sample can then be simulated and compared with experiment. Figure 2(b) shows the simulated analog for sample B, demonstrating that our simple model can qualitatively reproduce all of the trends in both FLN and PLE spectra. From the fitting procedure we extract single dot band-edge structures for each sample, shown in Fig. 7 without LO-phonon replicas. The position of band-edge absorption (solid line) and emission (dotted line) features are plotted relative to the energy of the emitting state. The three absorption features (α, β_1, and β_2) discussed above for sample G are also resolved in samples F and H. In smaller sizes (A–H) only two features (α and β) are observed. The model line shapes also indicate that with increasing size both the spacing between features and their linewidths decrease dramatically. Note the change in energy scale between samples A–D and E–H in Fig. 7.

For clarity Fig. 7 does not include LO-phonon coupling. Figure 8 shows the model absorption and emission line shapes for sample B including LO-phonon coupling. As in all of our samples the absorption coupling constant for this sample ($S_a=0.12$) is significantly smaller than the emission coupling constant ($S_e=0.45$). For the entire size series S_a ranges between 0.08 and 0.2, consistent with recent Raman studies,[32,33] which find S_a (the Huang-Rhys parameter) be-

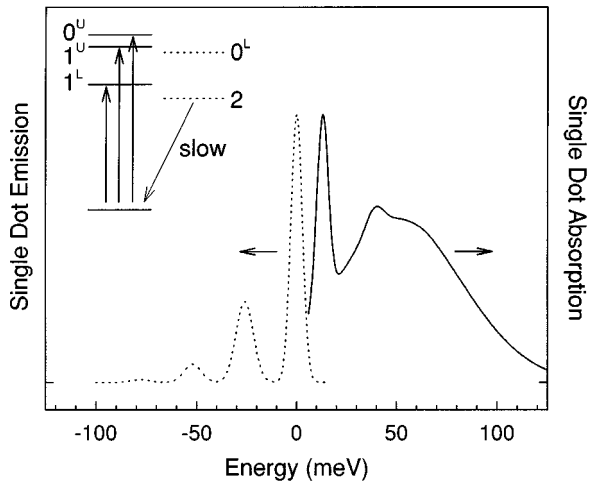

FIG. 8. Single dot absorption (solid line) and emission (dotted line) structure for sample B including LO-phonon coupling. An energy-level diagram illustrates the band-edge exciton structure. The sublevels are labeled by $|N_m|$ with superscripts to distinguish upper (U) and lower (L) sublevels with the same $|N_m|$. Optically active (passive) levels are shown as solid (dotted) lines.

tween 0.125 and 0.275 for CdSe QD's.[33] For the emitting state we find S_e between 0.36 and 0.5.

The complete set of model line-shape parameters for samples A–H, which describes quantitatively what Fig. 7 represents pictorially, is summarized in Table I. The band-edge absorption lines are described in terms of their separation from the emitting state (δ's), their relative oscillator strength (C's), and their linewidths (γ's). The increase in linewidth with decreasing size is consistent with previous results.[34,35] Below we discuss the size dependence of both the transition spacings and their relative oscillator strength.

IV. DISCUSSION

As shown in the preceding paper,[4] the size dependence of the broad featureless transitions in the optical spectra of CdSe QD's can be quantitatively described by effective mass models that include the complexity of the CdSe valence band.[5–9] For convenience these models assume spherical dots and work within the spherical band approximation,[36–38] since more sophisticated treatments have not been required to explain experimental results. In this case they predict that the band-edge exciton ($1S_{3/2}1S_e$) is eightfold degenerate. Recent theoretical work[10,11,13–16] has extended these models to include the effects of the hexagonal lattice,[10] the nonspherical shape,[11] and the electron-hole exchange interaction.[13–16] When these terms are considered, the initially eightfold degenerate band-edge exciton is split into five sublevels.[13–16] For the exchange interaction the important quantum number is the total angular momentum, $N=F_h+F_e$, where F_h (F_e) is the hole (electron) angular momentum. When the crystal field of the hexagonal lattice and/or the nonspherical shape are also included, the good quantum number is the projection of N along the unique crystal axis N_m. The five sublevels are then labeled by $|N_m|$: one sublevel with $|N_m|=2$, two with $|N_m|=1$, and two with $|N_m|=0$. Levels with $|N_m|>0$ are twofold degenerate.

This exciton fine structure is illustrated in an energy-level diagram in Fig. 8. The five sublevels are labeled by $|N_m|$ with superscripts to distinguish upper (U) and lower (L) sublevels with the same $|N_m|$. The lowest band-edge state, $|N_m|=2$, is forbidden in the electric dipole approximation and is referred to as the ''dark exciton.'' Relaxation of the electron-hole pair into this state can explain the long radiative lifetimes observed in CdSe QD's,[14–16] previously attributed to surface traps.[20,27,39–42] Since two units of angular momentum are required to return to the ground state from the $|N_m|=2$ sublevel, this transition is one-photon-forbidden. However, less efficient, phonon-assisted transitions can occur, explaining the stronger LO-phonon coupling of the emitting state (S_e) and the long radiative lifetimes (at 10 K).[16]

We have previously shown that band-edge absorption structure in TDA experiments is consistent with predicted band-edge exciton splittings.[18] We observed both narrow (α) and broad (β) absorption features in the TDA spectrum. Since the 0^L sublevel is optically passive [see Eq. (7) below],[16] α was assigned to the lowest allowed transition, 1^L, and β to a combination of 1^U and 0^U. The emitting state was assigned to the ''dark exciton.'' The assignment of β to a combination of 1^U and 0^U is further supported by the FLN-PLE results of this paper. In larger samples (F–H) β_1 and β_2 can be assigned to the individual 1^U and 0^U sublevels, previously unresolved.

To test these assignments we compare our experiments to

TABLE I. Effective radius and model line-shape parameters for samples A–H and TDA results. The integrated areas (C_t) are shown as percentages of the total band-edge oscillator strength.

Sample	a (Å)	S_a	S_e	δ_1 (meV)	δ_2 (meV)	δ_3 (meV)	C_1 (%)	C_2 (%)	C_3 (%)	$\gamma_{1,0}$ (meV)	$\gamma_{2,0}$ (meV)	$\gamma_{3,0}$ (meV)
A	15	0.1	0.5	17.7	65.4		10.9	89.1		4.0	42	
B	19	0.12	0.45	13.0	48.6		10.6	89.4		2.9	31	
C	21	0.1	0.36	8.4	43.4		8.6	91.4		2.5	32	
D	24	0.08	0.4	4.5	35.3		10.3	89.7		2.4	29	
E	27	0.12	0.7	1.5	29.5		7.8	92.2		1.8	20	
TDA[a]	30			2	26		17.9	82.1		1.7	14.4	
F	33	0.2	0.5	3.5	20.5	38.5	27.5	47.2	25.3	2.0	8.0	8.0
G	44	0.2	0.4	1.0	8.8	17.6	40.9	27.6	31.5	1.6	3.6	3.6
H	50	0.2	0.4	1.0	10.0	18.6	54.7	23.4	21.9	1.7	4.0	3.0

[a]TDA data from Ref. 18.

the calculated energies of the sublevels. The effects of the crystal field, the nonspherical shape, and the exchange interaction are included in perturbation theory. The net splitting (Δ) due to the internal crystal field (Δ_{int}) and shape asymmetry (Δ_{asym}) is

$$\Delta(\beta,\mu,a)=\Delta_{\text{int}}+\Delta_{\text{asym}}, \tag{4}$$

where β is the effective mass ratio of the bulk A and B bands along the ''c'' axis, a is the effective dot radius,[17] and $\mu=c/b-1$ where c (b) is the major (minor) dot axis.[10,11] The size-dependent exchange contribution can be written in terms of

$$\eta=\left(\frac{a_B}{a}\right)^3\hbar\omega_{\text{ST}}\chi, \tag{5}$$

where a_B is the exciton Bohr radius, $\hbar\omega_{\text{ST}}$ is the singlet-triplet splitting in the bulk A exciton due to exchange, and χ is a constant, which in CdSe equals 0.78.[16] In terms of Δ and η, the size-dependent energies of the five sublevels are[16]

$$\begin{aligned}\varepsilon_2&=-\frac{3\eta}{2}-\frac{\Delta}{2},\\ \left.\begin{matrix}\varepsilon_{1^U}\\ \varepsilon_{1^L}\end{matrix}\right\}&=\frac{\eta}{2}\pm\left(\frac{(2\eta-\Delta)^2}{4}+3\eta^2\right)^{1/2},\\ \left.\begin{matrix}\varepsilon_{0^U}\\ \varepsilon_{0^L}\end{matrix}\right\}&=\frac{\eta}{2}+\frac{\Delta}{2}\pm 2\eta.\end{aligned} \tag{6}$$

Figure 9(a) shows the size dependence of the calculated band-edge structure. For this calculation we use literature values for the bulk A-B splitting (25 meV),[43] $\hbar\omega_{\text{ST}}$ (0.13 meV),[44] a_B (56 Å),[9] μ,[45] and β (0.28).[4] The sublevels are plotted relative to the energy of 1^L. In large dots the sublevels converge to two fourfold degenerate states, analogous to the bulk A and B excitons. In this limit these two states are split by the combined effect of the crystal field and the nonspherical shape of the dot. As the size of the dot decreases the exchange interaction is enhanced due to quantum confinement and the sublevels fan out. Figure 9(b) shows the position of the absorbing (filled circles and squares) and emitting (open circles) features from Fig. 7 and TDA results,[18] relative to the narrow absorption feature α (1^L). For samples F–H both the positions of β_1 and β_2 (plusses) and their weighted average (squares) are shown. Comparison with theory indicates that the model accurately reproduces many aspects of the data. Both the splitting between $|N_m|=2$ and 1^L (the Stokes shift) and the splitting between 1^L and the upper states (1^U and 0^U) are described reasonably well. This result is particularly significant since, although the predicted structure strongly depends on the theoretical input parameters,[16] only literature values were used in the theoretical calculation.

The predicted structure in Fig. 9(a) also helps to understand why the 1^U and 0^U sublevels are not resolved in smaller dots (A–H). Previously we speculated that these features were much broader than 1^L due to a combination of

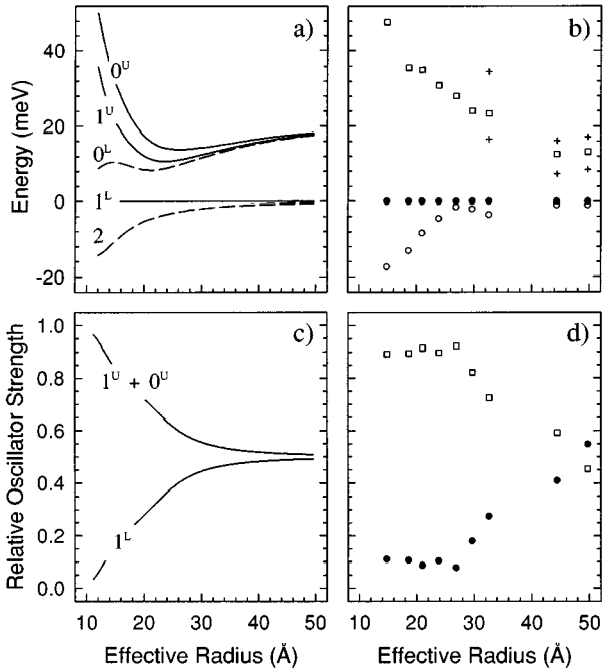

FIG. 9. (a) The calculated band-edge exciton ($1S_{3/2}1S_e$) structure vs effective radius. The sublevels are labeled by $|N_m|$ with superscripts to distinguish upper (U) and lower (L) sublevels with the same $|N_m|$. Positions are relative to 1^L. Optically active (passive) levels are shown as solid (dashed) lines. (b) Position of the absorbing (filled circles and squares) and emitting (open circles) features from Fig. 7 and TDA results from Ref. 18. In samples F–H both the positions of β_1 and β_2 (plusses) and their weighted average (squares) are shown. (c) Calculated relative oscillator strength of the optically allowed band-edge sublevels vs effective radius. The combined strength of 1^U and 0^U is shown. (d) Observed relative oscillator strength of the band-edge sublevels: 1^L (filled circles) and the combined strength of 1^U and 0^U (squares).

lifetime effects and inhomogeneous broadening.[18] Lifetime broadening occurs in 1^U and 0^U since these levels each have a rapid relaxation pathway via 1^L and 0^L, respectively, while 1^L can relax only through a much slower spin-flip mechanism. However, since we do not expect the lifetime of the upper states (1^U and 0^U) to increase with increasing size, this mechanism cannot explain the decrease in their linewidths in large dots. According to Fig. 9(a), inhomogeneous broadening can provide an explanation. The spacing between the emitting state and the upper states (1^U and 0^U) becomes less size dependent as the size is increased. Therefore, since size and shape distributions in our samples are fairly constant with size,[19] we expect inhomogeneous broadening of the upper states to decrease with size, becoming negligible in the largest dots. When this effect is combined with the general increase in homogeneous linewidth of all absorption and emission features with decreasing size,[34,35] it is not surprising that 1^U and 0^U are only resolved in the largest dots.

Further quantitative evidence for our assignments is obtained from the oscillator strengths of the optically allowed sublevels. Following the approach of Ref. 10 the transition probabilities for randomly oriented QD's can be written as

$$\left.\begin{matrix} P_{0^U} \\ P_{0^L} \end{matrix}\right\} = \frac{(1\pm 1)^2 K P^2}{9},$$
$$\left.\begin{matrix} P_{1^U} \\ P_{1^L} \end{matrix}\right\} = \frac{4KP^2}{9}\left(\frac{2\sqrt{f^2+d}\mp f\pm\sqrt{3d}}{2\sqrt{f^2+d}}\right), \tag{7}$$

where P is the Kane interband matrix element, $f=(-2\eta+\Delta)/2$, $d=3\eta^2$, and K is the square of the radial overlap integral

$$K=\frac{2}{a}\left|\int dr\ r\ \sin(\pi r/a)R_0(r)\right|^2, \tag{8}$$

where $R_0(r)$ is the hole radial function in the band-edge exciton ($1S_{3/2}1S_e$). Note that Eq. (7) predicts that 0^L is optically passive. In Fig. 9(c) the predicted oscillator strength of the optically active sublevels is shown. The strength of the upper states (1^U and 0^U) is combined since these states are not individually resolved in many of our samples. The experimental values are plotted in Fig. 9(d). Reasonable agreement between experiment and theory is observed, again with no fitting parameters.

To understand the size dependence of the oscillator strengths we consider two opposing limits. In large dots the states converge to A- and B-like excitons [as in Fig. 9(a)], each possessing half of the total band-edge oscillator strength. Therefore, we expect the relative oscillator strengths of 1^L and the combined upper states (1^U and 0^U) to each approach 0.5 in large sizes. In small dots the exchange interaction dominates and the crystal field and nonspherical shape effects become negligible. In this limit ($\Delta=0$) the sublevels converge to two states labeled by the total angular momentum N: an optically forbidden five fold degenerate $N=2$ state, and an optically allowed three fold degenerate $N=1$ state. Since 1^L is correlated to the $N=2$ state in the large exchange limit, we expect it to be only weakly allowed in small dots. 1^U and 0^U converge to the $N=1$ state and therefore carry nearly all of the oscillator strength.

The agreement between experiment and theory in Fig. 9 indicates that our FLN and PLE results support the predicted band-edge exciton fine structure. However, our results also demonstrate where theory may be improved. The model clearly fails to predict the observed splitting between 1^U and 0^U in large dots [Fig. 9(b)]. In this size regime theoretical levels have already converged to the A- and B-like excitons. While this discrepancy would appear to indicate that theory underestimates the exchange splitting, a change in this parameter would also affect the Stokes shift, which is well described by the model. Further theoretical work is required to address this issue.

In addition, since the presence of band-edge fine structure explains many optical properties previously explained by surface trapping of the carriers,[20,27,39–42] the role of the surface in the photophysics of these materials is now unclear. ''Surface effects'' had been argued to be important, especially in small dots, since a large fraction of the constituent atoms lie at the interface. Whether any discrepancies observed in Fig. 9 can be explained by the influence of the surface remains an open question.

V. CONCLUSION

We present photoluminescence excitation and fluorescence line narrowing results that exhibit structure within the first absorption feature of CdSe quantum dots. We study the size dependence of this structure by examining eight CdSe samples ranging from ~15 to ~50 Å in mean effective radius. Band-edge exciton splittings have been predicted as a result of the hexagonal lattice and nonspherical shape of our dots as well as the electron-hole exchange interaction. To compare with these theories we extract single dot absorption and emission line shapes from our data. We find that theory agrees well with the position and relative strengths of the absorption features in our model line shapes, supporting our previous claim that band-edge exciton fine structure is observed in these samples.

ACKNOWLEDGMENTS

We thank M. Nirmal for stimulating discussions and C. B. Murray and M. Kuno for assistance in sample preparation. D.J.N. benefited from support by NSF and Arthur D. Little. M.G.B. thanks the Lucille and David Packard Foundation and the Alfred P. Sloan Foundation for support. This work was funded in part by NSF (DMR-91-57491) and the NSF-MRSEC Program (DMR-94-00034). We also thank the MIT Harrison Spectroscopy Laboratory (NSF-CHE-93-04251) for use of its facilities.

*Present address: University of California, San Diego, 9500 Gilman Drive, La Jolla, CA 92093-0340.

[1] Al. L. Efros and A. L. Efros, Fiz. Tekh. Poluprovodn. **16**, 1209 (1982) [Sov. Phys. Semicond. **16**, 772 (1982)].

[2] L. E. Brus, J. Chem. Phys. **80**, 4403 (1984).

[3] For a review see L. E. Brus, Appl. Phys. A **53**, 465 (1991).

[4] D. J. Norris and M. G. Bawendi, preceding paper, Phys. Rev. B **53**, 16 338 (1996).

[5] J. B. Xia, Phys. Rev. B **40**, 8500 (1989).

[6] G. B. Grigoryan, E. M. Kazaryan, Al. L. Efros, and T. V. Yazeva, Fiz. Tverd. Tela **32**, 1772 (1990) [Sov. Phys. Solid State **32**, 1031 (1990)].

[7] K. J. Vahala and P. C. Sercel, Phys. Rev. Lett. **65**, 239 (1990); P. C. Sercel and K. J. Vahala, Phys. Rev. B **42**, 3690 (1990).

[8] S. W. Koch, Y. Z. Hu, B. Fluegel, and N. Peyghambarian, J. Cryst. Growth **117**, 592 (1992).

[9] A. I. Ekimov, F. Hache, M. C. Schanne-Klein, D. Ricard, C. Flytzanis, I. A. Kudryavtsev, T. V. Yazeva, A. V. Rodina, and Al. L. Efros, J. Opt. Soc. Am. B **10**, 100 (1993).

[10] Al. L. Efros, Phys. Rev. B **46**, 7448 (1992).

[11] Al. L. Efros and A. V. Rodina, Phys. Rev. B **47**, 10 005 (1993).

[12] C. B. Murray, D. J. Norris, and M. G. Bawendi, J. Am. Chem. Soc. **115**, 8706 (1993).

[13] T. Takagahara, Phys. Rev. B **47**, 4569 (1993); S. Nomura, Y. Segawa, and T. Kobayashi, *ibid.* **49**, 13 571 (1994).

[14] P. D. J. Calcott, K. J. Nash, L.T. Canham, M. J. Kane, and D. Brumhead, J. Lumin. **57**, 257 (1993).

[15] M. Chamarro, C. Gourdon, P. Lavallard, and A. I. Ekimov, Jpn. J.

Appl. Phys. Suppl. **34-1**, 12 (1995).
[16] M. Nirmal, D. J. Norris, M. Kuno, M. G. Bawendi, Al. L. Efros, and M. Rosen, Phys. Rev. Lett. **75**, 3728 (1995).
[17] Sizes reported are estimated from extensive size-dependent transmission electron microscopy (TEM) and small-angle x-ray measurements and are based on the energy of the first absorption peak. We report the effective radius of our prolate dots, defined as $a=[(b^2c)^{1/3}]/2$ where b and c are the short and long axes, respectively.
[18] D. J. Norris and M. G. Bawendi, J. Chem. Phys. **103**, 5260 (1995).
[19] C. B. Murray, Ph.D. thesis, Massachusetts Institute of Technology, 1995.
[20] M. G. Bawendi, W. L. Wilson, L. Rothberg, P. J. Carroll, T. M. Jedju, M. L. Steigerwald, and L. E. Brus, Phys. Rev. Lett. **65**, 1623 (1990).
[21] By single dot line shape we mean the line shape required by each dot in our model to reproduce the PLE and FLN results. The band-edge structure in this line shape may be an upper bound to the true structure if multiple inhomogeneities are present, not all of which are removed by experiment.
[22] W. Hoheisel, V. L. Colvin, C. S. Johnson, and A. P. Alivisatos, J. Chem. Phys. **101**, 8455 (1994).
[23] C. R. M. de Oliveira, A. M. de Paula, F. O. Plentz Filho, J. A. Medeiros Neto, L. C. Barbosa, O. L. Alves, E. A. Menezes, J. M. M. Rios, H. L. Fragnito, C. H. Brito Cruz, and C. L. Cesar, Appl. Phys. Lett. **66**, 439 (1995).
[24] P. A. M. Rodrigues, G. Tamulaitis, P. Y. Yu, and S. H. Risbud, Solid State Commun. **94**, 583 (1995).
[25] In addition to size, other inhomogeneities may influence the energy of the band edge exciton. We include these here in the descriptions ''smallest'' or ''largest.''
[26] D. J. Norris, Ph.D. thesis, Massachusetts Institute of Technology, 1995.
[27] M. Nirmal, C. B. Murray, and M. G. Bawendi, Phys. Rev. B **50**, 2293 (1994).
[28] S. Schmitt-Rink, D. A. B. Miller, and D. S. Chemla, Phys. Rev. B **35**, 8113 (1987).
[29] M. C. Klein, F. Hache, D. Ricard, and C. Flytzanis, Phys. Rev. B **42**, 11 123 (1990).
[30] Full luminescence is simulated by setting $A(v_{\rm exc},v')$ constant in Eq. (1).
[31] W. H. Press, B. P. Flannery, S. A. Teukolsky, and W. T. Vetterling, *Numerical Recipes in C* (Cambridge University Press, Cambridge, 1988), Chap. 14.
[32] J. J. Shiang, S. H. Risbud, and A. P. Alivisatos, J. Chem. Phys. **98**, 8432 (1993).
[33] J. J. Shiang, R. K. Grubbs, and A. P. Alivisatos (unpublished).
[34] D. M. Mittleman, R. W. Schoenlein, J. J. Shiang, V. L. Colvin, A. P. Alivisatos, and C. V. Shank, Phys. Rev. B **49**, 14 435 (1994); R. W. Schoenlein, D. M. Mittleman, J. J. Shiang, A. P. Alivisatos, and C. V. Shank, Phys. Rev. Lett. **70**, 1014 (1993).
[35] D. J. Norris, M. Nirmal, C. B. Murray, A. Sacra, and M. G. Bawendi, Z. Phys. D **26**, 355 (1993).
[36] N. O. Lipari and A. Baldereschi, Phys. Rev. Lett. **42**, 1660 (1970); A. Baldereschi and N. O. Lipari, Phys. Rev. B **8**, 2697 (1973).
[37] B. L. Ge'lmont and M. I. D'yakonov, Fiz. Tekh. Poluprovodn. **5**, 2191 (1971) [Sov. Phys. Semicond. **5**, 1905 (1972)].
[38] In the spherical band approximation only terms of spherical symmetry in the Luttinger Hamiltonian are considered in first order.
[39] M. O'Neil, J. Marohn, and G. McLendon, J. Phys. Chem. **94**, 4356 (1990).
[40] A. Eychmüller, A. Hässelbarth, L. Katsikas, and H. Weller, Ber. Bunsenges. Phys. Chem. **95**, 79 (1991).
[41] A. Hässelbarth, A. Eychmüller, and H. Weller, Chem. Phys. Lett. **203**, 271 (1993).
[42] M. G. Bawendi, P. J. Carroll, W. L. Wilson, and L. E. Brus, J. Chem. Phys. **96**, 946 (1992).
[43] *Semiconductors. Physics of II-VI and I-VII Compounds, Semimagnetic Semiconductors*, edited by K. H. Hellwege, Landolt-Börnstein, New Series, Group III, Vol. 17, Pt. b (Springer-Verlag, Berlin, 1982).
[44] V. P. Kochereshko, G. V. Mikhailov, and I. N. Ural'tsev, Fiz. Tverd. Tela **25**, 769 (1983) [Sov. Phys. Solid State **25**, 439 (1983)].
[45] Size-dependent aspect ratio measurements from Ref. 19 are fit to a polynomial.